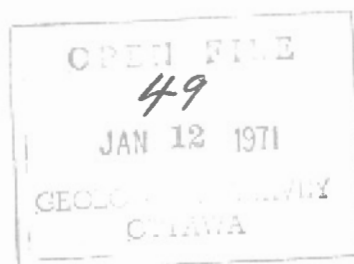


COMPACTION AND FLUID MIGRATION  
IN CRETACEOUS SHALES  
OF WESTERN CANADA

by

Kinji Magara

June 1970



This document was produced  
by scanning the original publication.

Ce document est le produit d'une  
numérisation par balayage  
de la publication originale.

## CONTENTS

	<u>Page</u>
ABSTRACT	A-1
<u>Part I.</u> Shale Porosity Distribution and Fluid Pressure in Alberta and Saskatchewan Subsurface	I-1
1.   Introduction	I-1
2.   Shale Porosity - Depth and Fluid Pressure - Depth Relations	I-2
<u>Part II.</u> Porosity-Permeability Relationship of Shale	II-1
1.   Introduction	II-1
2.   Fluid-Pressure Gradients and Movements of Fluids in Shales	II-2
3.   Shale Porosity-Permeability Relationship in Western Canada	II-6
4.   Comparison of Log-Derived and Laboratory- Derived Porosity-Permeability Relations	II-8
<u>Part III.</u> Causes of Abnormal Pressures	III-1
1.   Introduction	III-1
2.   Expulsion of Fluids from Shales during Subsidence	III-2
3.   Clay-Mineralogical Alteration	III-9
<u>Part IV.</u> Amounts of Fluids Expelled From Cretaceous Shales in British Columbia and Northwestern Alberta	IV-1
1.   Introduction	IV-1
2.   Porosity Distributions of Cretaceous Shales	IV-2

CONTENTS (continued)

	<u>Page</u>
<u>Part V.</u> Compaction Experiment Using Clays	V-1
1.    Introduction	V-1
2.    Apparatus for Compaction Experiment	V-1
3.    Method of Experiment	V-2
4.    Results of Experiments	V-3
 <u>Part VI.</u> Trend of Future Research	 VI-1
1.    Introduction	VI-1
2.    Volume of Fluids Expelled Downward and Upward	VI-1
3.    Shale-Porosity Distribution as an Indicator for Permeability of Reservoir Rocks	VI-3

## ABSTRACT

Part I: Shale-porosity distributions within Cretaceous and Tertiary rocks of the Alberta and Saskatchewan subsurface have been determined by the use of sonic and formation-density logs, and the examination of cores and surface rock samples. At shallow depths, shale porosity appears to be exponentially related to depth. Porosity at depth in Cretaceous shales, especially in the western part of the area studied, tends to be greater than the porosity-depth trend established at shallower depths would suggest, and is related to anomalously high fluid-pressure conditions. Thus, abnormally high fluid pressures may be expected where shales are incompletely compacted.

Part II: Fluid-pressure gradients in shales can be determined by the porosity distribution, as derived from sonic logs, of incompletely compacted shales. Differing permeabilities in shales may be estimated through use of the fluid-pressure gradient and Darcy's law. Calculated shale permeabilities and porosity values can be integrated to establish a relationship between shale porosity and permeability in the subsurface. This method of analysis applied to Cretaceous shales in the subsurface of Alberta and Saskatchewan reveals that in shale the permeability increases less with increase in porosity than the amount given by Archie's relation, which is based on sandstones and carbonate rocks. This calculated porosity-permeability relationship for shales has been verified in numerous other studies by laboratory-measured porosity and permeability data.

Part III: Anomalously high pressures in the deep subsurface can be explained by fluid-release mechanisms related to compaction of shales.

The volume of fluids which should be expelled from shales in unit time to reach compaction equilibrium may be determined for several different rates of sedimentation, based on the shale-porosity data in western Canada. For each rate of sedimentation or subsidence there is a minimum permeability for reaching compaction equilibrium, which may be calculated according to Darcy's law. Comparison of this calculated minimum permeability with actual shale permeabilities, determined by laboratory measurements, suggests that at relatively shallow depths shale should usually be permeable enough to permit compaction equilibrium to be attained, and to maintain normal hydrostatic pressure. At depth, however, actual permeabilities are less than the calculated minimum necessary for compaction equilibrium, so that abnormal pressures may occur at these greater depths. The incidence of such abnormal pressures should increase with increases in the rate of sedimentation and in the total thickness of the sequence.

Part IV: Shale-porosity distribution in incompletely compacted shale zones may also be affected by the permeability of adjacent sandstone or carbonate rock bodies. Sharp decrease of porosity in shales close to such rock bodies would suggest that relatively large volumes of fluids have been expelled from the shales into the adjacent sandstones or carbonates. If this expelled fluid volume is large, the possibility of hydrocarbon accumulation in such sandstone or carbonate rocks is considered to be strong. To illustrate such a study, Cretaceous shales associated with hydrocarbon reservoirs in the subsurface of northwestern Alberta and northeastern British Columbia have been examined. Most Mesozoic oil and gas pools in this area are concentrated where a greater volume of fluids is considered to have been expelled downward from the overlying shales.

Part V: In order to obtain laboratory data on compaction and fluid-expulsion relationships, a number of experiments were conducted on several kinds of clays. The results yielded porosity distributions similar to those of Cretaceous shales in the subsurface of western Canada.

Part VI: In order to understand the fluid-migration history in a given area, porosity patterns of incompletely compacted shales can be constructed for several stages of compaction. In part VI, these relationships are investigated and some suggestions made for future work.

## ACKNOWLEDGMENTS

This work was carried out between August 1967 and August 1969 at the Institute of Sedimentary and Petroleum Geology of the Geological Survey of Canada in Calgary, Alberta. The project was supported by a Post-Doctorate Fellowship from the National Research Council. The author wishes to express his appreciation for the advice and supervision provided by Dr. D.J. MacLaren, Director of the Institute, and Dr. D.K. Norris, head of the Structural Geology Section. Drs. R.G. MacCrossan, R.W. Macqueen, C.J. Yorath and R.M. Procter, also of the Institute, provided research assistance and helpful comment, as did Dr. Brian Hitchon of the Research Council of Alberta in Edmonton. Mr. G.M. Peterkin of the Institute constructed the apparatus for the compaction experiments. Miss J.B. Greig of Imperial Oil Limited contributed editorial advice.

Part I. SHALE-POROSITY DISTRIBUTION  
AND FLUID PRESSURE  
IN ALBERTA AND SASKATCHEWAN SUBSURFACE

1. Introduction

Shale-porosity distributions of Cretaceous and Tertiary rocks of the Alberta and Saskatchewan subsurface have been determined by means of sonic and formation-density logs. More than 160 wells have been examined for this purpose. Shale cores of a few wells have also been studied in order to check the relation between log-derived porosity and laboratory-measured porosity. Surface rock samples have been collected and their porosity values determined in the laboratory.

As the writer, along with Brian Hitchon\*, plans to publish the complete findings later elsewhere,\*\* this paper does not include all of the work. The plan of Part I is to indicate several examples of the shale-porosity distributions in the Alberta and Saskatchewan subsurface, and to show the relation between porosity distribution and fluid pressure.

---

\* Research Council of Alberta, Edmonton, Alberta, Canada

\*\* Bulletin of Canadian Petroleum Geology



## 2. Shale Porosity - Depth and Fluid Pressure - Depth Relations

More than 160 wells, all with sonic logs, have been studied in the subsurface of western Canada (Fig. 1). In 13 of these wells both sonic and formation-density logs have been run (Table 1). Because the formation-density log provides both density and porosity values, a relationship between porosity and acoustic-transit time can be determined by using data from both logs. Figure 2 shows the relation between shale porosity,  $\phi$ , derived from formation-density logs, and shale-transit time,  $\Delta t_{\text{shale}}$  ( $\mu$  sec/ft), from sonic logs in the Cretaceous and Tertiary rocks of the area studied. Determination of shale porosity is based on the assumption that the grain density of the shales equals 2.65 gm/cc.

After numerous laboratory tests, Wyllie et al., (1956, 1958) concluded that, in consolidated strata with uniformly distributed small pores, there is a linear relation between porosity and transit time:

$$\Delta t_{\log} = \phi \cdot \Delta t_{\text{liquid}} + (1 - \phi) \Delta t_{\text{matrix}} \quad \dots (1)$$

or

$$\Delta t_{\log} = (\Delta t_{\text{liquid}} - \Delta t_{\text{matrix}}) \phi + \Delta t_{\text{matrix}} \quad \dots (1')$$

where  $\Delta t_{\log}$  is transit time on sonic log,  $\Delta t_{\text{liquid}}$  and  $\Delta t_{\text{matrix}}$  are transit times in formation liquid and matrix respectively, and  $\phi$  is formation porosity. This equation means that, in rock of uniform lithology, transit time increases with porosity.

According to Figure 2 there is a linear relation between shale porosity,  $\phi$ , and shale-transit time,  $\Delta t_{\text{shale}}$  ( $\mu$  sec/ft), in the Cretaceous and Tertiary shales studied. The function obtained by the least-squares method is as follows,

$$\phi = 0.00472 \times \Delta t_{\text{shale}} - 0.362 \quad \dots (2)$$

By using equation (2), the transit-time data from sonic logs can be converted to estimated porosity values.

For convenience, groups of wells close to each other have been considered as a single well, and in this paper these groups are named A, B, ....., Y (Fig. 1). The vertical porosity distributions of Cretaceous and Tertiary shales at these locations have been determined by the use of sonic logs. The main purpose of Part I, however, is to compare the shale-porosity distributions and fluid-pressure profiles. Several examples of shale-porosity distributions are therefore shown in Figure 3 (the names of the wells used in this figure are listed in Table 2).

According to the shale-porosity plots of Figure 3, shale-porosity values decrease with depth, and on the semi-log paper porosity-depth relations within relatively shallow depths are closely approximated by straight lines. At greater depths, however, the trend deviates toward higher porosity values.

Figure 3 also shows the fluid pressure - depth relations derived from the oil and gas wells in the same area. These pressure data are from both well completions and drill-stem tests (Oil and Gas Conservation Board, 1967).

In the zones of abnormally high shale porosity in Figure 3, the fluid pressure is higher than the hydrostatic, although the pressure data are derived from the different kinds of rock - sandstones or carbonates.

Hubbert and Rubey (1959) have demonstrated that the load,  $S$ , is supported jointly by the fluid pressure,  $p$ , and the grain-to-grain bearing strength,  $\sigma$ , of the clay aggregates:

$$S = \sigma + p, \quad \dots(3)$$

and load  $S$  can be expressed

$$S = \bar{\rho}_{bw} \cdot g \cdot Z \quad \dots(4)$$

where  $\bar{\rho}_{bw}$  is the mean value of the water-saturated bulk density of the overlying sediments,  $g$  is the acceleration of gravity, and  $Z$  is the depth of burial.

The grain-to-grain bearing stress,  $\sigma$ , exerted by the porous clay depends solely on the degree of compaction. The stress  $\sigma$  increases continuously as the porosity decreases (Rubey and Hubbert, 1959):

$$\sigma = f(\phi). \quad \dots(5)$$

If the shale porosity  $\phi$  is abnormally high or the stress  $\sigma$  is abnormally low, the fluid pressure  $p$  should be abnormally high in order to support the overburden load  $S$  (equations 4 and 5).

Figure 3 shows that the shale-porosity distribution in western Canada is useful for predicting abnormal pressure.

The determination of abnormal pressure in this case may be explained by means of the typical distribution of the vertical porosity of the shale, shown in Figure 4. A hydrostatic-pressure environment prevails at shallow depths and an abnormal pressure at depth. The "normal porosity trend" line is drawn through the general average of the values plotted for the zone of hydrostatic pressure. When the porosity is plotted on the logarithmic scale and the depth on the arithmetic scale, the "normal porosity trend" line is commonly straight, because of an exponential function between depth and porosity for the hydrostatic-pressure condition\*.

---

\* Rubey and Hubbert (1959), equation (15)

$$f = f_0 \cdot e^{-CZ},$$

where  $f$  is the shale porosity at depth  $Z$ ,  $f_0$  the shale porosity when  $Z=0$ ,  $e$  the base Napierian Logarithms, and  $C$  an exponential factor of dimension (length)<sup>-1</sup>.

As explained previously, the shale-porosity values in the abnormal-pressure zone are greater than the values the "normal porosity trend" would indicate. If the porosity of shale at depth  $Z$  in the abnormal-pressure zone is equal to that at depth  $Z_e$  on the "normal porosity trend" line, the grain-to-grain bearing strength is the same for both shales (see Fig. 4).

The overburden load,  $S_e$ , and the fluid (hydrostatic) pressure,  $p_e$ , at depth  $Z_e$  can be shown as follows:

$$S_e = \bar{\rho}_{bw} \cdot g \cdot Z_e \quad \dots (6)$$

$$p_e = \rho_w \cdot g \cdot Z_e \quad \dots (7)$$

where  $\rho_w$  is the density of the formation water.

The function between the load, the strength of the clay and the fluid pressure at  $Z_e$  is shown as follows (see equation 3):

$$S_e = \sigma_e + p_e$$

or

$$\sigma_e = S_e - p_e \quad \dots (8)$$

Then, when equations (6) and (7) are introduced into equation (8), we obtain

$$\begin{aligned} \sigma_e = S_e - p_e &= \bar{\rho}_{bw} \cdot g \cdot Z_e - \rho_w \cdot g \cdot Z_e \\ &= (\bar{\rho}_{bw} - \rho_w) g \cdot Z_e \quad \dots (9) \end{aligned}$$

(see Rubey and Hubbert, 1959, equation 10). Similarly, the overburden load  $S$  at depth  $Z$  is shown as equation (4)\*. As explained previously,

---

\* The writer assumes that the mean water-saturated bulk density of the overlying sediments for depth  $Z$  approximates that for depth  $Z_e$ .

the bearing strength  $\sigma$  at depth  $Z$  equals  $\sigma_e$  at depth  $Z_e$  in the hydrostatic-pressure zone, or

$$\sigma = \sigma_e. \quad \dots(10)$$

From equations (3), (4), (9) and (10) the fluid (abnormal) pressure  $p$  at depth  $Z$  can be shown as:

$$\begin{aligned} p &= S - \sigma = S - \sigma_e \\ &= \bar{\rho}_{bw} \cdot g \cdot Z - (\bar{\rho}_{bw} - \rho_w)g \cdot Z_e \\ &= \rho_w \cdot g \cdot Z_e + \bar{\rho}_{bw} \cdot g (Z - Z_e) \end{aligned} \quad \dots(11)$$

or

$$p(\text{psi}) = 0.44 \times Z_e(\text{ft}) + 1.0 \times (Z - Z_e) (\text{ft}). \quad \dots(11')$$

By using equation (11) or (11'), the shale-porosity distribution can be converted to the fluid-pressure distribution.

The curved broken lines in the fluid-pressure sections of Figure 3 show the possible maximum fluid pressures in shales as determined by the porosity distributions. The actually measured pressures in the reservoirs are sometimes lower than the maximum values derived from the shales. This can be explained by the greater permeability values in the reservoirs.

## Part II. POROSITY-PERMEABILITY RELATIONSHIP OF SHALE

### 1. Introduction

In discussing fluid movements in shales during compaction, a knowledge of shale permeability is essential. If the relationship between permeability and porosity can be determined, such discussion of fluid movements in a shale column will become easier, for several porosity-depth relations have already been proposed for shales (Athy, 1930; Hedberg, 1936; Dickinson, 1953; Weller, 1959). There is, however, very little literature on the permeability-porosity relationship of shales (see Bredehoeft and Hanshaw, 1968). This is probably because: (1) most oil companies do not want to take any permeability data in shales because of their low economic importance; (2) it is quite difficult to measure reasonable permeability values for shales, because while their original permeability tends to be low, well cores (shale) may have some cracks or fissures caused by drilling that would increase it; (3) it is not possible to estimate shale permeability in the subsurface by producing an appreciable amount of fluid from wells, because shales normally produce no fluid.

Methods of estimating formation-fluid pressure by well logs (Hottmann and Johnson, 1965; MacGregor, 1965; Wallace, 1965; Foster and Whalen, 1966; Fons and Holt, 1966; Rogers, 1966), which have been developed in the last few years, are based on an intimate relation between pore-fluid pressure and shale compaction or shale porosity. (The writer has discussed this subject in Part I.) The study to be discussed here shows that the fluid-pressure gradient in incompletely compacted shales can also be determined by the porosity distribution. It is possible, therefore, to determine permeability changes in shales by using the fluid-

pressure gradients and Darcy's law.

Having done this, the writer intends to estimate the permeability changes of Cretaceous shales in Alberta and Saskatchewan subsurface in this manner, then to combine shale porosity with permeability in order to investigate the relation between them.

## 2. Fluid-Pressure Gradients and Movements of Fluids in Shales

As discussed in Part I, the value of abnormal fluid pressure at depth  $Z$  in the incompletely compacted shales as shown in Figure 4 is given as follows:

$$p = \rho_w \cdot g \cdot Z_e + \bar{\rho}_{bw} \cdot g \cdot (Z - Z_e). \quad \dots(11)$$

This equation means that the abnormal pressure  $p$  at depth  $Z$  is equivalent to (the hydrostatic pressure at  $Z_e$ ) + (the overburden pressure between  $Z_e$  and  $Z$ ).

The abnormal fluid-pressure  $p$  can be expressed as follows (Hubbert and Rubey, 1959, equation 133):

$$p = p_n + p_a \quad \dots(12)$$

where  $p_n$  is the normal or hydrostatic pressure and  $p_a$  a superposed anomalous pressure;  $p_n$  is expressed as:

$$p_n = \rho_w \cdot g \cdot Z. \quad \dots(13)$$

From equations (11), (12) and (13) the anomalous pressure (pressure above

the hydrostatic pressure)  $p_a$  can be shown to be:

$$\begin{aligned} p_a &= p - p_n = \rho_w \cdot g \cdot Z_e + \bar{\rho}bw \cdot g(Z - Z_e) - \rho_w \cdot g \cdot Z \\ &= (\bar{\rho}bw - \rho_w)(Z - Z_e) \cdot g. \end{aligned} \quad \dots(14)$$

When, for convenience of description, we use a term  $h$  for  $(Z - Z_e)$  (Fig. 4), we can express this simply as:

$$p_a = (\bar{\rho}bw - \rho_w) \cdot g \cdot h. \quad \dots(15)$$

Then

$$\frac{dp_a}{dz} = [(\bar{\rho}bw - \rho_w)g] \frac{dh}{dz}. \quad \dots(16)$$

Now, let us discuss the values of  $\frac{dh}{dz}$  in the typical incompletely compacted shales, illustrated in Figure 5. As shown there,  $\frac{dh}{dz}$  is zero at point 0, where the tangential line on the porosity curve in the incompletely compacted shales is parallel to the "normal porosity trend" line. This is expressed as follows:

$$\left(\frac{dh}{dz}\right)_0 = 0.$$

At point  $a$ , at which the tangential line is vertical,  $\frac{dh}{dz}$  equals 1. This is similarly shown as:

$$\left(\frac{dh}{dz}\right)_a = 1.$$

Above point  $a$ ,  $\frac{dh}{dz}$  increases upward and its value is greater than 1, or

$$\left(\frac{dh}{dz}\right)_u > 1.$$

Below point 0,  $\frac{dh}{dz}$  has negative values and decreases downward. Somewhere below point 0, there must exist a point where  $\frac{dh}{dz}$  equals -1 (point  $b$  in Fig. 5), or

$$\left(\frac{dh}{dz}\right)_b = -1.$$



Below point  $b$ ,  $\frac{dh}{dz}$  values are given as follows:

$$\left(\frac{dh}{dz}\right)_d < -1.$$

In the equations above,  $0$ ,  $a$  and  $b$  denote the points  $0$ ,  $a$  and  $b$ , respectively, and  $u$  and  $d$  denote the points in the upward and downward fluid-movement zones in the incompletely compacted shales.

As explained above,  $\frac{dh}{dz}$  has a positive value above point  $0$  and a negative below. As the value of  $(\rho_{bw} - \rho_w)g$  in equation (16) is always positive,  $\frac{dpa}{dz}$  has a positive value above point  $0$  and a negative below. Fluid would move upward above point  $0$  and downward below. The volume of the upward fluid movement  $qu$  crossing unit area normal to the flow direction in unit time is given by Darcy's law:

$$qu = -\frac{ku}{\mu u} \left(\frac{dpa}{dz}\right)_u = -\frac{ku}{\mu u} (\rho_{bw} - \rho_w)g \left(\frac{dh}{dz}\right)_u, \quad \dots (17)$$

where  $ku$  and  $\mu u$  are respectively the permeability of shale and the viscosity of water at point  $u$  in the upward zone. As stated above,  $\frac{dh}{dz}$  at point  $a$  equals  $1$  (see Fig. 5). Hence, the volume of fluid movement  $qa$  at point  $a$  is given as follows:

$$\begin{aligned} qa &= -\frac{ka}{\mu a} \left(\frac{dpa}{dz}\right)_a = -\frac{ka}{\mu a} (\rho_{bw} - \rho_w)g \left(\frac{dh}{dz}\right)_a \\ &= -\frac{ka}{\mu a} (\rho_{bw} - \rho_w)g \quad \dots (18) \end{aligned}$$

In this case,  $qu$  and  $qa$  have negative values, and the following relation would exist:

$$qu \leq qa. \quad \dots (19)$$

From equations (17), (18) and (19) we obtain:

$$\frac{k_a}{k_u} \leq \frac{\mu_a}{\mu_u} \left( \frac{dh}{dz} \right)_u. \quad \dots (20)$$

As clearly seen in Figure 5, the porosity value at point  $a$  is maximum in the incompletely compacted shale zone, and the porosity decreases upward and downward. Supposing that there is a function between porosity and permeability of shale, and that the permeability decreases with decrease in porosity, the permeability value at point  $a$  would be greatest in this zone.

According to equation (20), the permeability ratio  $k_a/k_u$  can be calculated if the viscosity  $\mu_a$  and  $\mu_u$  of the formation fluid and  $\left( \frac{dh}{dz} \right)_u$  are known. It is possible to read the porosity values at the points  $a$  and  $u$ . Hence, the integration of the permeability values based on equation (20) with the porosity values is considered to be used to establish a relation between shale porosity and permeability in the subsurface.

The volume of fluid movement  $q_d$  in the downward zone is expressed as:

$$q_d = -\frac{k_d}{\mu_d} \left( \frac{dp_a}{dz} \right)_d = -\frac{k_d}{\mu_d} (\bar{\rho} b w - \rho_w) g \left( \frac{dh}{dz} \right)_d, \quad \dots (21)$$

where  $d$  denotes a point below point  $b$  in the downward fluid-movement zone.

As the value of  $\frac{dh}{dz}$  at point  $b$  equals -1, the amount  $q_b$  is shown as:

$$q_b = -\frac{k_b}{\mu_b} \left( \frac{dp_a}{dz} \right)_b = \frac{k_b}{\mu_b} (\bar{\rho} b w - \rho_w) g. \quad \dots (22)$$

In this case  $q_d$  and  $q_b$  have positive values and the following relation would exist:

$$q_d \geq q_b. \quad \dots (23)$$

From equations (21), (22) and (23) we obtain

$$\frac{kb}{kd} \leq -\frac{\mu b}{\mu d} \left( \frac{dh}{dz} \right)_d, \quad \dots (24)$$

where  $\left( \frac{dh}{dz} \right)_d$  is always negative. The right-hand side of equation (24) is, therefore, positive

$$\left( \frac{\mu b}{\mu d} > 0 \right).$$

Equation (24) as well as equation (20) can be used to obtain the permeability ratio of shale in the subsurface. The integration of the permeability values based on equation (24) with the porosity values is also used to establish a relation between shale porosity and permeability in the subsurface. The actual calculations in the Cretaceous shales in western Canada will be discussed in the next section.

### 3. Shale Porosity-Permeability Relationship in Western Canada

A porosity-permeability relationship of Cretaceous shales in Alberta and Saskatchewan subsurface will now be discussed, based on the method described above.

The "normal porosity trends" of shales in this area have been established in Part I (Fig. 3). According to this figure, the "normal porosity trend" tends to shift to smaller values from east to west in the area (shale porosity on the "normal porosity trend" at the same depth decreases from east to west, although the slope of the "trend" is almost constant). This decrease is attributed to the existence of a greater thickness of sediments in the western part in the geological past, which produced more compaction, and may be accounted for by the

removal of a greater thickness of the uppermost part of the sedimentary column in the west. After the erosion thickness has been compensated, the standard "normal porosity trend" in this area is determined and is shown in Figure 6. The function of the standard "normal porosity trend" of Cretaceous and Tertiary shales in the area studied is expressed as follows:

$$\begin{aligned}\phi &= 0.6 \times e^{-0.000588z(ft)} \\ &= 0.6 \times e^{-0.0000193z(cm)}. \quad \dots(25)\end{aligned}$$

The values of  $\frac{dh}{dz}$  based on the "normal porosity trend" in western Canada are illustrated in Figure 7. By using this figure,  $\frac{dh}{dz}$  values in the incompletely compacted shale zones are easily determined.

Now let us read the  $\frac{dh}{dz}$  values in the incompletely compacted shales in the Alberta and Saskatchewan subsurface (Fig. 1A). For this purpose, 35 wells, some of which are shown in Figures 8 and 9, have been chosen in the area where the Cretaceous formations have incompletely compacted shales.

The viscosity of the formation water would change mainly with temperature. The writer assumes that the average geothermal gradient in this area is 1.8° F per 100 feet of depth, and that the subsurface temperature at 2,000 ft. is 75° F, based on the temperature-depth data in Alberta (Oil and Gas Conservation Board, 1967, Fig. 10). The viscosity of the formation water at each depth based on this temperature data is determined, assuming that the dissolved-solid content of water equals 40,000 mg/l (see also Pirson, 1963, Fig. 4-6). The ratios  $ka/ku$  and  $kb/kd$  are calculated by equations (20) and (24) respectively, and the porosities  $\phi_a$ ,  $\phi_u$ ,  $\phi_b$ , and  $\phi_d$  at these points are read.

Figure 11 shows the plots of  $ka/ku$  or  $kb/kd$  (logarithmic scale) against  $\phi_a - \phi_u$  or  $\phi_b - \phi_d$  (arithmetic scale), when the equal signs in equations (20) and (24) are established. The average relation in this case is shown as a curved solid line. The actual  $ka/ku$  or  $kb/kd$  values, however, according to equations (20) and (24), would be smaller than these plotted values. The relation between  $ka/ku$  or  $kb/kd$  and  $\phi_a - \phi_u$  or  $\phi_b - \phi_d$  would, therefore, be expressed by the shadowed area in Figure 11.

Archie (1950) has proposed the porosity-permeability relationship for sandstones, limestones and muddy sands. According to it, an increase in porosity of about 3 per cent produces a tenfold increase in permeability. Archie's relation is shown as a straight line in Figure 11, where the increase of shale permeability with increase in porosity is less than that given by Archie's relation, which is based on sandstones and carbonate rocks.

#### 4. Comparison of Log-Derived and Laboratory-Derived Porosity-Permeability Relations

Data on permeability-porosity relations of shale are at present very scarce: Bredehoeft and Hanshaw (1968) have compiled some of what are available. The Geological Survey of Japan have measured the permeabilities and porosities of the mudstone cores of several stratigraphic test wells in Japan, and the writer has obtained similar data on a well in the Strathmore gas field in Alberta. The data for Japan and Alberta are listed in Table 3; they are also shown in Figure 12.

In Figure 12, Archie's porosity-permeability relation, mentioned above, is shown as a straight broken line (Archie), and Kozeny's (based

on sandstones) is shown as a curved broken line (Kozeny). The log-derived porosity-permeability relation in western Canada, when the equal signs in equations (20) and (24) are established, is illustrated as a curved solid line (Cretaceous shale). The actual relation could be shown by the shadowed area in Figure 12. The starting point for these three lines (Archie, Kozeny, and Cretaceous shale) in this figure is located at the point of porosity 0.2 (or 20%) and permeability  $3 \times 10^{-3}$  md. Although the data are derived from several different areas, Figure 12 would show that the log-derived porosity-permeability relation is more applicable for shales than are the Archie and Kozeny relations.

### Part III. CAUSES OF ABNORMAL PRESSURES

#### 1. Introduction

In the previous parts, an intimate relationship between shale porosity and fluid pressure has been discussed. This part deals with several causes of abnormal pressure.

Reservoir pressures in the subsurface usually approximate hydrostatic pressure, which equals the weight of the water column from reservoir to surface. A pressure that materially exceeds the weight of an equivalent column of water is "abnormal", and a pressure materially less is "subnormal" (Levorsen, 1954). Reservoir pressure will not exceed the weight of the overlying rock column, or geostatic pressure.

Dickinson (1951) reported an instance of abnormal pressure in the Gulf Coast equal to 0.87 times the geostatic, and Kok and Thomeer (1955) cited an example of 0.90 times. More data on abnormal pressures have been compiled by Rubey and Hubbert (1959). Dickinson (1951) also reported the first recognized association of abnormal pressures with the relative proportions of sand and shale in a geologic column. Abnormal pressures can be influenced also by the mean formation permeability, the elapsed time since deposition, the rate of deposition, and the amount of overburden (Hottmann and Johnson, 1965).

According to Thomeer and Bottema (1961), favorable conditions for abnormal pressures below shale columns may be found in younger sedimentary basins where the rapid deposition of thick shales over considerable areas did not allow time for hydrostatic equilibrium to be reached. With respect to the common occurrence of abnormal pressures in more deeply buried shale successions, Rubey and Hubbert (1959) advanced the

following explanation: "When the rate of sedimentation is somewhat greater, pore water may still escape rapidly enough to maintain an essentially hydrostatic pressure in the relatively porous mudstone at shallow and intermediate depths but not in the more compacted and therefore less permeable rock at greater depths". In a significant recent contribution, Powers (1967) advanced a new interpretation of the origin of abnormal fluid pressure in the deep subsurface, based on the application of current knowledge of clay-colloid chemistry and mineralogy. According to Powers, the alteration of montmorillonite to illite begins at a depth of about 6,000 feet and continues at an increasing rate to a depth usually about 9,000-10,000 feet, where no montmorillonite is left. The alteration offers a mechanism for desorbing the last few layers of bound water in clay and transferring it as free water to interparticle locations. These last few layers of bound water have a considerably greater density than free water, and water increases in volume as it is desorbed from between unit layers. As the water expands, it increases the pore-fluid pressure to abnormally high levels.

The writer also intends here to discuss qualitatively and quantitatively several possible explanations of abnormal fluid-pressure in the relatively deeper parts of sedimentary sequences.

## 2. Expulsion of Fluids from Shales during Subsidence

Let us assume a clay or shale sequence in which the clay or shale has reached a compaction equilibrium and within which the fluid pressure is hydrostatic (Stage A of Fig. 13). Additional sediments are added above this sequence in the marine condition and the sequence subsides an amount,



$l$ , in a time interval,  $t$ . If the entire shale reaches a new equilibrium condition of compaction after the subsidence of  $l$ , a porosity distribution such as shown by stage B in Figure 13 would be established. As explained in Parts I and II, an exponential function exists between shale porosity and depth at the equilibrium condition in western Canada.

Suppose that an outlet for fluid expulsion exists only at the surface, and the fluid is expelled upward. In this case the compaction of the shale from stage A to B would occur from the shallower to the deeper part of the sequence (Fig. 14). This figure shows schematically that the porosity decrease occurs from the shallower part to the deeper (from 1 to 5). In considering fluid migration under this circumstance, the fluid-pressure gradient between stages A and B must be determined, and Figure 15 has been constructed for this purpose. In this situation, the fluid-pressure difference  $P_l$  between depth  $Z$  on the stage B line (hydrostatic pressure) and depth  $Z + l$  on the stage A line (abnormal pressure) is given as:

$$P_l = S_l = \rho_{bwo} \cdot g \cdot l, \quad \dots (26)$$

where  $S_l$  is the overburden increase in this case and  $\rho_{bwo}$  is the water-saturated bulk density of shale at the surface (below sea level). When the fluid-pressure increase is resolved into two components (Hubbert and Rubey, 1959, equations 133 and 134),

$$P_l = P_{ln} + P_{la}$$

or

$$P_{la} = P_l - P_{ln}, \quad \dots (27)$$

where  $P_{ln}$  is the normal or hydrostatic pressure increase and  $P_{la}$  a superposed anomalous pressure increase. In this case  $P_{ln}$  is shown as

$$Pl_n = \rho_w \cdot g \cdot l. \quad \dots(28)$$

From equations (26), (27) and (28),  $Pl_a$  can be expressed as follows:

$$Pl_a = (\rho_{bwo} - \rho_w)g \cdot l \quad \dots(29)$$

or

$$\frac{Pl_a}{l} = (\rho_{bwo} - \rho_w)g. \quad \dots(30)$$

The anomalous pressure gradient in the situation shown in Figure 15 is given by equation (30).

Fluid movement in this case is shown by Darcy's law (see also equation 17):

$$q = \frac{k}{\mu} \frac{Pl_a}{l}, \quad \dots(31)$$

where  $q$  is a volume of water crossing unit area normal to the flow direction in unit time,  $k$  the permeability of shale, and  $\mu$  the fluid viscosity. The volume of water  $q_1$  passing depth  $Z_1$  in unit time in a shale column is expressed from equations (30) and (31) as

$$q_1 = \frac{k_1}{\mu_1} \frac{Pl_a}{l} = \frac{-k_1}{\mu_1} (\rho_{bwo} - \rho_w)g, \quad \dots(32)$$

where the subscript 1 denotes depth  $Z_1$ , and  $q_1$  is considered to be the volume of water passing through the shale at depth  $Z_1$ , whose permeability is  $k_1$ . The volume of the passing water  $Q_1$  in time interval  $t$  is given as

$$Q_1 = q_1 \cdot t = \frac{-k_1}{\mu_1} (\rho_{bwo} - \rho_w)g \cdot t. \quad \dots(33)$$

Assuming that the shale compaction occurs simply by the expulsion of fluids from the shales, the porosity difference in Figure 15 would indicate the amount that should be expelled between stages A and B for

the new equilibrium of compaction to be reached. Supposing that the direction of fluid expulsion in this case is upward, the amount that should pass through the shale at depth  $Z_1$  could be calculated.

An exponential function between shale porosity and depth at the equilibrium condition of compaction proposed by Rubey and Hubbert (1959, equation 15) is as follows:

$$\phi = \phi_0 \cdot e^{-CZ}, \quad \dots(34)$$

where  $\phi$  is the value of shale porosity at depth  $Z$ ,  $\phi_0$  the porosity when  $Z=0$ ,  $e$  the base Napierian logarithms, and  $C$  a constant of dimension (length) $^{-1}$ . The line of the stage A in Figure 15 could be shown mathematically by equation (34). Suppose that the subsidence  $l$  occurs in time interval  $t$  and the shales reach a new equilibrium condition of compaction (Stage B in Fig. 15). The porosity-depth relation in this case is shown as

$$\phi + \phi_l = \phi_0 \cdot e^{-C(Z + l)}, \quad \dots(35)$$

where  $\phi_l$  is the porosity difference between stage A and B. From equations (34) and (35),

$$\phi_l = \phi_0 \cdot e^{-CZ} (e^{-Cl} - 1). \quad \dots(36)$$

In this case the total amount of porosity decrease in a shale column with the unit base area is given by the integral of equation (36) as follows:

$$\int \phi_l dz = \phi_0 (e^{-Cl} - 1) \int e^{-CZ} dz. \quad \dots(37)$$

This amount of the porosity decrease is here considered to be the volume of fluids that should be expelled from the shale column for the new equilibrium to be reached. As this volume normally tends to go upwards,

the volume that should pass through depth  $Z_1$  for the equilibrium is expressed as

$$\int_{Z_1}^Z \phi_l dz = \phi_o (e^{-cZ} - 1) \int_{Z_1}^Z e^{-cZ} dz. \quad \dots (38)$$

$Z$  in equation (38) is considered to be the bottom depth of the shale sequence.

When this volume is equal to or less than  $Q_1$  in equation (33), sufficient fluids would be expelled from the shales and a hydrostatic-pressure environment would be established. When it is greater than  $Q_1$ , on the other hand, some fluids would remain and an abnormal pressure would occur. In the case where this volume is balanced with  $Q_1$  in equation (33), the following relation would exist:

$$Q_1 = -\frac{k_1}{\mu_1} (\rho_{bwo} - \rho_w) g \cdot t = \phi_o (e^{-cZ} - 1) \int_{Z_1}^Z e^{-cZ} dz. \quad \dots (39)$$

In this equation  $k_1$  is considered to be the minimum permeability for the new compaction equilibrium to be reached, and is given as

$$k_1 = \frac{\mu_1 \cdot \phi_o}{(\rho_{bwo} - \rho_w) g \cdot t} (1 - e^{-cZ}) \int_{Z_1}^Z e^{-cZ} dz. \quad \dots (40)$$

If the average subsidence or sedimentation rate in time interval  $t$  is given as  $\Delta Z$ , the following relation would exist:

$$Z = t \cdot \Delta Z. \quad \dots (41)$$

When we take a certain time interval (for example, 1 second) for  $t$  in equations (40) and (41), we can calculate  $k_1$  at several sedimentation rates.

Using equations (40) and (41), the minimum permeability for compaction equilibrium can be determined for several rates of sedimentation  $\Delta z$ . Calculations have been made on the assumption that  $\rho_{bwo}$  and  $\rho_w$  in the area studied are 1.67 and 1.02 (gm/cc) respectively.  $\phi_o$  is assumed to be 0.60 (60%). The viscosity of the formation water is determined from the temperature data in the plains (see Fig. 10). The minimum permeabilities for compaction equilibrium when the sedimentation rate  $\Delta z$  is  $10^{-7}$ ,  $10^{-8}$ ,  $10^{-9}$  and  $10^{-10}$  cm/sec are illustrated in Figure 16, in which the permeability is plotted on the logarithmic scale (ordinate) and the porosity on the arithmetic scale (abscissa). In this case the bottom depth of the shale sequence is infinite. The depth scale corresponding to the shale-porosity value on the standard "normal porosity trend" (Fig. 6) is also shown on the abscissa. In Figure 16, the laboratory-measured porosity and permeability data of shales and clays from Table 3 or Figure 12 are also plotted. As explained previously, these porosity and permeability data were obtained from several different formations in different areas, which means that this porosity-permeability relation does not represent one particular area, but could be used to arrive at a general porosity-permeability relationship for shale. Such a relationship could, therefore, be shown by the shadowed area in Figure 16.

In this figure, the minimum-permeability line when  $\Delta z = 10^{-8}$  cm/sec intersects the actual permeability zone between 0.27 (or 27%) porosity and 0.09 (or 9%) porosity. The porosity values correspond to depths of about 1,300 ft. and 3,200 ft. respectively, on the standard "normal porosity trend" of western Canada. In depths shallower than 1,300 ft. (or porosity greater than 0.27), the actual permeability would be greater than the minimum for compaction equilibrium to be reached, when the sedimentation rate  $\Delta z$  equals  $10^{-8}$  cm/sec. In this case, enough fluid

for the equilibrium could be expelled from the shale and a hydrostatic-pressure condition would be established. In the deeper depth, on the contrary, the actual permeability would be less than the minimum for equilibrium. Some fluids would remain in this part of the sequence and an abnormal pressure would occur.

Figure 17 is a plot of the possible tops of the abnormal pressures at several sedimentation rates; it shows that when the rate of sedimentation is high the abnormal pressures would occur at relatively shallow depths.

The previous discussions are based on the assumption that the bottom of the shale sequence exists at an infinite depth, or  $Z = \infty$ , in equation (40). However, what would happen if the bottom lay at a relatively shallow depth with an impermeable base? Figure 18 shows the minimum permeability vs. depth when the bottom depth  $Z = 3,000$  ft.,  $4,000$  ft.,  $10,000$  ft. and  $\infty$  ( $\Delta Z = 10^{-8}$  cm/sec). According to this figure, the minimum permeability for equilibrium at the same depth would increase as the bottom depth  $Z$  increases. This means that the thicker the entire shale sequence, the greater the possibility of abnormal pressures developing.

In the Cretaceous formations of western Canada, the abnormal pressures occur mostly in the western parts of the plains (Fig. 3), where the thickness of the entire formations is greater than in the east and sedimentation would have been more rapid. This high sedimentation rate and great total thickness are, therefore, considered to be possible causes of the abnormal pressures in this part of the plains.

### 3. Clay-Mineralogical Alteration

In order to examine the possibility of so-called montmorillonite dehydration proposed by Powers (1967), the writer obtained data on the clay-mineral contents of several well cores. Although most of his findings will, however, be reserved for the joint paper with Brian Hitchon, one example in western Canada will be given here.

Figure 19 shows the data on core porosity, sonic porosity and mineral content of shales. Figure 19A is the shale-core porosity-depth relation of the Strathmore 7-12-25-25W4 well in Alberta (Fig. 1). The porosity is calculated from the dry density of the cores, assuming that the grain density of the shales equals 2.65 gm/cc. Because this well does not have any sonic-log data, the closest well in which a sonic log was run (Arden 6-4-25W4) has been chosen for comparison (Fig. 19B). Figure 19B shows the porosity-depth relation of this well based on the shale porosity -  $\Delta t$  relation in the plains (Fig. 2). In this case both core and sonic porosities fit fairly well. According to Figures 19A and B, abnormally high shale porosities exist below about 800 ft.

The results of clay-mineralogical studies of the Strathmore cores, made by A.E. Foscolos at the Geological Survey of Canada, Calgary, are given in order of abundance of several clays (Table 4). The right-hand picture of Figure 19 shows this result more understandably. At 1,000 ft.  $\pm$  the order of abundance of montmorillonite seems to drop and kaolinite seems to increase. Illite, however, does not increase at this depth.

The shale compaction study for western Canada has estimated the thickness of the eroded formations in the geological past to be about 1,400 ft. at this location. (This also will be included in the joint paper with Brian Hitchon). The maximum depth to the top of montmorillonite

increase would have been 2,400 ft.† at this location. This estimated depth is considered to be much shallower than the depth of montmorillonite dehydration proposed by Powers (1967).



Part IV. AMOUNT OF FLUIDS EXPELLED FROM CRETACEOUS SHALES  
IN BRITISH COLUMBIA AND NORTHWESTERN ALBERTA

1. Introduction

Shale compaction would occur mainly by the expulsion of fluids from the shales. In the previous three parts, the writer has discussed the relation between shale compaction, fluid migration, and several shale properties. Shale compaction could, however, be influenced by adjacent permeable rocks such as sandstones and carbonates. This problem has been discussed on the basis of well-log data in Nagaoka Plain, Japan (Magara, 1968a). According to this paper on the Japanese Tertiary rocks, sharp porosity decreases occur in the shales close to the permeable reservoir rocks. Such decreases may therefore be used as indicators for the permeabilities of the adjacent reservoir rocks. The difference in porosity between the initial and the present stage would indicate the volume of fluids expelled from the shales to the reservoir rocks in the geological past. As it is considered that a certain percentage of these fluids would have been the source of petroleum, the discussion on this volume would be quite useful and important for petroleum exploration.

This part of the paper discusses the amount of fluids expelled downward from the Cretaceous shales to the reservoir rocks in British Columbia and the northwestern part of Alberta. This particular area has been chosen because of the incompletely compacted shales in the Cretaceous formations and the various hydrocarbon pools in the Cretaceous and adjacent formations.

## 2. Porosity Distributions of Cretaceous Shales

About 300 wells, all with sonic logs, have been chosen in this area (Fig. 20); their names are listed in Table 5. Shale porosity of the Cretaceous formations has been determined from the sonic-log data by using the relation of porosity and transit time as shown in Figure 2. The vertical shale-porosity distributions along lines A-A', B-B', C-C', D-D', E-E', F-F', and G-G' (Fig. 20) are shown respectively in Figures 21, 22, 23, 24, 25, 26 and 27.

As explained in the previous parts, the abnormally high-porosity (or incompletely compacted) shale is normally associated with abnormally high fluid-pressure. In a vertical shale column, the fluid would move from a point of higher anomalous pressure (higher excess pressure over the hydrostatic) to a point of lower anomalous pressure. The directions of fluid migration in a schematic shale-porosity distribution have been discussed in Part II (see Fig. 5).

The curved broken lines in Figures 21-27 indicate the boundary surfaces between upward and downward fluid migration in the shales. This boundary surface is determined by the idea developed in Part II; below it, the fluid would move downward to the reservoirs. The thickness of the downward-migration zone normally increases westward. Sharp porosity decreases in the shales close to the reservoir rocks occur mostly in the western part of the area, suggesting that the underlying reservoirs have relatively higher permeabilities and the fluid would have migrated to them relatively easily from the shales. In the eastern parts, on the contrary, such porosity decreases are not clear, suggesting that the underlying reservoirs have relatively lower permeabilities, if the other conditions are the same.

The objective of this study is to calculate the volume of fluid expelled downward from the shales to the underlying reservoir rocks. As a first step, however, the isopach map of the downward-migration zone in the shales (Fig. 28) has been constructed; this map also shows locations of oil and gas pools in the underlying reservoirs (Lower Cretaceous, Jurassic and Triassic formations). According to Figure 28, most of these oil and gas pools are in the area where the downward-migration zone is thicker than 500 ft.

A method of calculating the volume of fluid expelled in the geological past has been developed (Magara, 1968a), and is used in this part of the paper.

Assuming that the shale grain before and after burial is the same, the following relation obtains:

$$V(1 - \bar{\phi}) = V'(1 - \bar{\phi}'), \quad \dots(42)$$

where  $V$  and  $V'$  are the respective shale volumes, and  $\bar{\phi}$  and  $\bar{\phi}'$  the respective average porosity values, before and after burial. First, the present (after burial) vertical porosity distribution of shale, as shown schematically in Figure 29, is established. In calculating the volume of the downward migration, the present (after burial) volume  $V'$  of the downward-migration zone per unit vertical column of the shales, and the present average porosity  $\bar{\phi}'$  of the zone, are necessary.

We have, however, no idea about the porosity distribution at any time in the geological past (before burial). The writer assumes that this porosity distribution conformed to the "normal porosity trend" of the shales, implying that at that time fluid could be expelled from the shales rather easily and a hydrostatic pressure prevailed. By assuming a "normal porosity trend" for the porosity distribution before burial,

the average porosity  $\bar{\phi}$  in this zone is known. The shale volume  $V$  (before burial) is given as,

$$V = V' \frac{(1 - \bar{\phi}')}{(1 - \bar{\phi})}. \quad \dots (43)$$

A volume of fluid expelled downward,  $Wd$ , can be calculated as,

$$Wd = \Delta\bar{\phi} \cdot V = (\bar{\phi} - \bar{\phi}') V' \frac{(1 - \bar{\phi}')}{(1 - \bar{\phi})}. \quad \dots (44)$$

This method is applied to the area studied.

Figure 30 shows the volume of fluid expelled downward from the Cretaceous shales to the underlying reservoir rocks, as well as the locations of oil and gas pools in the underlying reservoirs. Most oil and gas pools are concentrated in the area where the greater volume of fluid is considered to have been expelled from the shales to the reservoirs.

The previous discussions have taken into account only the volume of the downward migration from the overlying shales to the reservoirs. Upward migration from the underlying source rocks might also have had some role in the formation of hydrocarbons in the reservoirs. It is believed, however, that hydrocarbons produced from the overlying shales could have been entrapped in the reservoirs more effectively because the overlying shales are also important as cap rock, but it is doubtful that the cap rock overlying the reservoirs was present at the time the fluids from the underlying shales were expelled upward. The overlying source shales thus seem to be more important in hydrocarbon accumulation, and the study was therefore confined to them.

## Part V. COMPACTION EXPERIMENT USING CLAYS

### 1. Introduction

So far several porosity patterns in the Cretaceous and Tertiary shales in western Canada have been discussed. These porosity patterns could be affected by the clay-mineral content of shale, the properties of the formation fluids, and the presence of adjacent permeable rocks (sandstones and carbonates). Several compaction experiments have been conducted on clays and the results reported (Chilingar and Knight, 1960, Meade, 1966, Engelhardt and Gaida, 1963). Most of these works, however, were concerned with the compaction of clays and the changes of water salinity during compaction, and hence used relatively small specimens. They are, therefore, not suitable for determining the porosity distributions inside the clay.

The objective of the present experiments is to obtain porosity patterns in several clays at several stages of compaction. An apparatus for this purpose was constructed by the Geological Survey of Canada in Calgary.

### 2. Apparatus for Compaction Experiment

Figure 31 shows the apparatus that was devised for the compaction experiments. It is composed of a metal base (a) and a 2"-diameter brass tube (b) divided into ten 2" segments. Brass plates (c) are welded to the top and bottom of each segment: the brass bolts (d), which hold the segments together, permit the removal of individual segments, and rubber rings between the segments prevent water leakage. Metal plates (e) are also placed between the segments, and they are used for slicing the clays.

Above the ten segments is a cylinder (f), containing a brass piston (g) with a rubber tip. The piston may be systematically loaded at (h) to a maximum weight of 400 lbs. In experimental compaction, the cylinder and the ten segments are filled with water-saturated clays of various compositions. During progressive loading, water is expelled through the top (i) and bottom (j) outlets. Two sandstone cores are placed at the top and bottom of the clays.

### 3. Method of Experiment

The inner volume and the empty weight of each segment (B) are first measured. After a segment has been filled with water-saturated clay, it is weighed again; the difference in weight then would be the weight of the water-saturated clay. The bulk density  $\rho_{bw}$  of the clay can then be determined by dividing this weight by the inner volume of the segment. Porosity is calculated by using the following equation,

$$\rho_{bw} = \phi \cdot \rho_w + (1 - \phi) \cdot \rho_g$$

or

$$\phi = \frac{\rho_g - \rho_{bw}}{\rho_g - \rho_w}, \quad \dots (45)$$

$\rho_g$  of the clays is assumed to be 2.65 gm/cc. The initial porosity of clays in each segment is calculated by equation (45). Following this, the ten segments, a metal base, a cylinder and a piston are put together. The piston is loaded to a weight of 400 lbs.

When compaction has taken place and water is expelled from the clays, the ten segments are removed and the weight of each, including the clays, is measured. Porosity distribution at this stage is determined.

Repeating such measurements, porosity patterns at different stages of compaction can be determined. New clays are added at the top of the clays (in the cylinder), and compaction experiments proceed.

#### 4. Results of Experiments

##### A: Montmorillonite\*:

Both top and bottom outlets are open, simulating the presence of permeable sandstones above and below a shale sequence. The clay was saturated with about 1.5N NaCl solution. Results are shown in Figure 32. Big porosity decreases occur at both ends, close to the outlets; decrease in the middle, on the other hand, is relatively slow.

##### B: Montmorillonite\*:

This time, the bottom outlet is closed, simulating impermeability of the underlying sandstone (Fig. 33). A big porosity decrease occurred at the uppermost part of the clay, close to the top outlet. Between stages 2 and 3, the height of the piston was measured periodically; the results are shown in Figure 34. There seems to be an exponential function between piston height and time, indicating that the compaction slows down with time.

##### C: Montmorillonite\*:

Six segments from the bottom were initially filled with salt-water-saturated (2N NaCl) montmorillonite, while the cylinder and four segments from the top were filled with fresh-water-saturated montmorillonite (Fig. 35). This simulates deposition in saline-water conditions followed by

---

\* Montmorillonite No. 25,  
John C. Lane Tract,  
(Bentonite)  
Upton, Wyoming

fresh-water conditions. More water was expelled from the bottom or salt-water side, than from the top or fresh-water side. In other words, in this situation more water was squeezed out downward than upward.

D: Kaolinite\*\*:

In this case the top and bottom outlets were open (Fig. 36). The bulk density or porosity difference is relatively small.

E: Montmorillonite-Kaolinite:

Seven segments from the bottom were initially filled with kaolinite, and the cylinder and three segments from the top with montmorillonite (Fig. 37). This time both top and bottom ends were open. In segments 4 and 5, the porosity increased from stage 1 to stages 2 and 3. This is because the montmorillonite, which has a higher porosity, was pushed down during this experiment.

F: Illite\*\*\*:

The results for illite are shown in Figure 38. The porosity difference under this weight (400 lb.) is very small.

G: Montmorillonite-Illite:

The results here are shown in Figure 39. In this case the major porosity difference occurred in montmorillonite. Porosity in the illite part is small at stage 1 and very little change occurred during the experiments.

---

\*\* Kaolinite No. 4  
Macon, Georgia

\*\*\* Illite No. 35  
Fithian, Illinois, 48W1535



## Part VI. TREND OF FUTURE RESEARCH

### 1. Introduction

In Part IV the volume of fluids expelled downward from the Cretaceous shales to the underlying reservoir rocks was calculated. This method would be practically useful for petroleum exploration, because if this volume is large, the possibility of hydrocarbons is considered to be great accordingly. In this calculation, the writer assumes that the initial porosity distribution conforms to the present "normal porosity trend". However, this is not necessarily true in every case, although the semi-quantitative volume of fluids expelled in the geological past might tell something about the possibility of finding oil and gas, and the properties of the reservoir rocks, such as permeability.

In order to discuss the volume of fluids expelled, the porosity patterns of incompletely compacted shales at several stages of compaction should be known. In other words, the compaction process in incompletely compacted shales should be clearly understood. Once we know this process, we could calculate the volume of fluids expelled during a certain geological time.

### 2. Volume of Fluids Expelled Downward and Upward

The log-derived porosity-permeability relationship is shown by the shadowed area in Figure 11 (Part II). This means that the present study could not obtain a single function between shale porosity and permeability, but obtained some range between them. However, the relationship

between  $\frac{\mu a}{\mu u} \left( \frac{dh}{dz} \right)_u$  or  $-\frac{\mu b}{\mu d} \left( \frac{dh}{dz} \right)_d$  in equations (20) and

(24) and  $(\phi a - \phi u)$  or  $(\phi b - \phi d)$  can be expressed as a single curved line (Fig. 40). By using this figure and Figure 7, the slopes of the shale-porosity curves at each  $(\phi a - \phi u)$  or  $(\phi b - \phi d)$  are determined. This means that the ideal shale-porosity curves in the incompletely compacted shale zone can be constructed by Figures 40 and 7.

Figure 41 shows such examples of the constructed porosity distributions (A:  $\phi a = 0.6$  or 60%; B:  $\phi a = 0.5$  or 50%; C:  $\phi a = 0.4$  or 40%; D:  $\phi a = 0.3$  or 30%; E:  $\phi a = 0.2$  or 20%.) The values of  $\frac{\mu a}{\mu u}$  and  $\frac{\mu b}{\mu d}$  are assumed in this case to be 1 ( $\mu a = \mu u$ , or  $\mu b = \mu d$ ). Superposition of the curves in Figure 41 may suggest the porosity distribution at several stages of compaction, but the porosity differences in the upward and downward fluid-movement zones, from one stage to another, must fit the volumes of fluid expelled upward and downward between these stages.

The ratio  $qu/qd$  is expressed as follows (see equations 17 and 21):

$$\frac{qu}{qd} = \frac{ku}{kd} \cdot \frac{\mu d}{\mu u} \cdot \frac{\left( \frac{dh}{dz} \right)_u}{\left( \frac{dh}{dz} \right)_d} , \quad \dots (46)$$

Supposing that  $\left( \frac{dh}{dz} \right)_u$  and  $\left( \frac{dh}{dz} \right)_d$  values are taken at the points of the same porosity value in both upward and downward zones (Fig. 42) and the permeability values of two shales are the same when porosity values are the same, equation (46) is reduced to

$$\frac{qu}{qd} = \frac{\mu d}{\mu u} \cdot \frac{\left( \frac{dh}{dz} \right)_u}{\left( \frac{dh}{dz} \right)_d} , \quad \dots (47)$$

The ratio of the volumes of upward and downward fluid movement can be determined by equation (47).

The values of  $qu/qd$  when the maximum porosity  $\phi_a$  equals 0.6, 0.5, ... 0.2 are determined from Figure 41 and equation (47) and the average values are shown in Figure 43 ( $qu/qd - \phi_a$  relationship). Figure 43 shows a general tendency of  $qu/qd$  to decrease with a decrease in  $\phi_a$ . This means that the relative volume of the downward fluid-movement against the upward increases with compaction of the shales.

Figure 44 shows a superposition of the porosity curves, in which the porosity differences in the upward and downward fluid-movement zones between two stages of compaction fit these  $qu/qd$  ratios. The area between two curves may show the volumes of fluids expelled from the unit shale column during these two stages of compaction. The area above line 0-0' represents the volume of upward fluid expulsion, the area below the volume of downward expulsion. The volumes per unit vertical shale column, whose base area is 1 ft.<sup>2</sup>, are also shown in Figure 44.

The superposition of the porosity curves at several stages of compaction is here based on the shale-compaction study. To get such porosity patterns of each particular area and formation, the superposition should be based on the data from the area and formation, when the volumes of upward and downward migrations from shales to a reservoir can be calculated for this particular area. This work will be left for the future.

### 3. Shale-Porosity Distribution as an Indicator for Permeability of Reservoir Rocks

According to the discussions in Part II, the slope of the porosity curve in the incompletely compacted shale zone would indicate the anomalous fluid-pressure gradient in the shales. The integration of this pressure gradient and Darcy's law may reveal something about the permeability of the adjacent rocks.

Figure 45 is constructed to explain this situation. The left-hand side is a schematic shale-porosity distribution, in which incompletely compacted shales exist in the deeper part. Suppose that fluid is expelled upward from the sequence: in this situation, the volume of fluids,  $q$ , passing vertically through the sequence would gradually increase upward (see the right-hand side of Fig. 45). Because this increase is considered to be quite gradual, we may obtain an instant idea of the average permeability of the rocks by the porosity distribution of the shales. According to Darcy's law, the following relation exists,

$$q = -\frac{k}{\mu} \cdot \frac{d\rho a}{dz}. \quad \dots (50)$$

In zones A, C and E of Figure 45,  $\frac{dh}{dz}$  values (see Fig. 7) are relatively large and hence  $\frac{d\rho a}{dz}$  would be relatively large. In zones B and D, on the other hand,  $\frac{dh}{dz}$  values are relatively small, and  $\frac{d\rho a}{dz}$  would also be relatively small. Because the changes of  $q$  and  $\mu$  in this case are quite gradual, a large  $\frac{d\rho a}{dz}$  will produce a small  $k$  value in equation (50) and vice versa. Low  $\frac{dh}{dz}$  values (B and D) may, therefore, be associated with high average permeabilities. In zones of B and D, the shales may have a higher permeability than those in A, C, and E, or some intercalation of such permeable rocks as sandstones and carbonate rocks may exist in B and D. In any event, the shale-porosity distribution can be used as an instant indicator of the average permeability of rocks. This is also a problem for the future.

## REFERENCES

- ARCHIE, G. E., 1942 - The electrical resistivity log as an aid in determining some reservoir characteristics: Am. Inst. Min. Metall. Eng. Trans., v. 146, p. 54-62.
- \_\_\_\_\_ 1950 - Introduction to petrophysics of reservoir rocks: Am. Assoc. Petroleum Geologists Bull., v. 34, no. 5, p. 943-961.
- ATHY, L. F., 1930 - Density, porosity, and compaction of sedimentary rocks: Am. Assoc. Petroleum Geologists Bull., v. 14, no. 1, p. 1-24.
- BREDEHOEFT, J. D. and HANSHAW, B. B., 1968 - On the maintenance of anomalous fluid pressures: I, thick sedimentary sequence: Geol. Soc. America Bull., v. 79, No. 9, p. 1097-1106.
- BURST, J. F., 1969 - Diagenesis of Gulf Coast clayey sediments and its possible relation to petroleum migration: Am. Assoc. Petroleum Geologists Bull., vol. 53, no. 1, p. 73-93.
- CHILINGAR, G. V. and KNIGHT, L., 1960 - Relationship between pressure and moisture content of kaolinite, illite and montmorillonite clays: Am. Assoc. Petroleum Geologists Bull., vol. 44, no. 1, p. 101-106.
- DICKINSON, G., 1951 - Geological aspects of abnormal reservoir pressures in the Gulf Coast region of Louisiana, U.S.A.: 3rd World Petroleum Congress Proc., Sec. 1, p. 1-16; 1953, Am. Assoc. Petroleum Geologists Bull., v. 37, no. 2, p. 410-432.
- ENGELHARDT, W. von, and GAIDA, K. H., 1963 - Concentration changes of pore solutions during the compaction of clay sediments: Jour. Sed. Petrology, v. 33, p. 919-930.
- FONS, L. AND HOLT, O. 1966 - Formation log pressure data can improve drilling: World Oil, v. 163, no. 4, p. 70-74.
- FOSTER, J. B., et al, 1966 - Estimation of formation pressures from electrical surveys - offshore Louisiana: Jour. Petroleum Technology, v. 18, no. 2, p. 165-171.
- HANSHAW, B. B. and BREDEHOEFT, J. D., 1968 - On the maintenance of anomalous fluid pressures: II, source layer at depth: Geol. Soc. America Bull., v. 79, no. 9, p. 1107-1122.
- HEDBERG, H. D., 1936 - Gravitational compaction of clays and shales: Am. Jour. Science, v. 31, no. 4, p. 241-287.

- HOTIMANN, C. E., and JOHNSON, R. K., 1965 - Estimation of formation pressures from log-derived shale properties: Jour. Petroleum Technology, v. 17, no. 6, p. 717-722.
- HUBBERT, M. K., 1953 - Entrapment of petroleum under hydrodynamic conditions: Am. Assoc. Petroleum Geologist Bull., v. 37, no. 8, p. 1954-2026.
- \_\_\_\_\_ and RUBEY, 1959 - Role of fluid pressure in mechanics of overthrust faulting, I: Geol. Soc. America Bull., v. 70, no. 2, p. 115-166.
- KOK, P. C., and THOMEER, J. H. M. A., 1955 - Abnormal pressures in oil and gas reservoirs: Geologie en Mijnbouw, Aug.
- LEVORSEN, A. I., 1954 - Geology of petroleum: San Francisco, W. H. Freeman Co., 703 p.
- MacGREGOR, J. R., 1965 - Quantitative determination of reservoir pressures from conductivity log: Am. Assoc. Petroleum Geologists Bull., v. 49, no. 9, p. 1502-1511.
- MAGARA, K., 1968 - Compaction and migration of fluids in Miocene mudstone, Nagaoka Plain, Japan: Am. Assoc. Petroleum Geologists Bull., v. 52, no. 12, p. 2466-2501.
- \_\_\_\_\_ 1968 - Subsurface fluid pressure profile, Nagaoka Plain, Japan: Japan Petroleum Institute Bull., vol. 10, p. 1-7.
- MEADE, R. H., 1966 - Factors influencing the early stages of the compaction of clays and sands: Review, Jour. Sedimentary Petrology, vol. 36, p. 1085-1101.
- OIL and GAS CONSERVATION BOARD, 1967 - Pressure-depth and temperature-depth relationships, Alberta crude oil pools, OGCB-67-22, Calgary, Alberta.
- PIRSON, S. J., 1963 - Handbook of well log analysis: N. J., Prentiss-Hall, Englewood Cliffs.
- POWERS, M. C., 1967 - Fluid-release mechanisms in compacting marine mud-rocks and their importance in oil exploration: Am. Assoc. Petroleum Geologists Bull., v. 51, p. 1240-1253.
- ROGERS, L. C., 1966 - How Shell controls Gulf Coast pressures: Oil and Gas Jour., v. 64, no. 20, p. 264-266.

RUBEY, W. W. and HUBBERT, M. K., 1959 - Role of fluid pressure in mechanics of overthrust faulting, II: Geol. Soc. America Bull., v. 70, p. 167-206.

THOMEER, J. H. M. A., and BOTTEMA, J. A., 1961 - Increasing occurrence of abnormally high reservoir pressures in boreholes, and drilling problems resulting therefrom: Am. Assoc. Petroleum Geologists Bull., v. 45, no. 10, p. 1721-1730.

WALLACE, W. E., 1965 - Logs measure abnormal susurface pressures: Oil and Gas Jour., v. 63, no. 27, p. 102.

WELLER, J. M., 1959 - Compaction of sediments, Am. Assoc., Petroleum Geologists Bull., vol. 43, no. 2, p. 273-310.

WYLLIE, M. R. J., et al, 1956 - Elastic wave velocities in heterogeneous and porous media: Geophysics, v. 21, no. 1, p. 41-70.

---

et al, 1958 - An experimental investigation of factors affecting elastic wave velocities in porous media: Geophysics, v. 23, no. 3, p. 459-493.